Primljen / Received: 25.6.2023.
Ispravljen / Corrected: 23.4.2024.
Prihvaćen / Accepted: 5.7.2024.
Dostupno online / Available online: 10.11.2024.

Physical and mechanical properties of weathered sandstone rock-like materials under freeze-thaw cycles

Authors:

Zhang Zhen, MSc. CE
Qinghai University, Xining, China
Faculty of Civil Engineering
symzoro@163.com

Assoc.Prof. **Wang Qingzh**, PhD. CE
Qinghai University, Xining, China
Faculty of Civil Engineering
Ministry of Transport, Xining, China
Laboratory for technology of highway construction and maintenance in the permafrost region
wangqingzhi87@qhu.edu.cn
Corresponding author

Zhang Kui, MSc. CE
Qinghai University, Xining, China
Faculty of Civil Engineering
2020990090@qhu.edu.cn

Prof. **Fang Jianhong**, PhD. CE
Ministry of Transport, Xining, China
Laboratory for technology of highway construction and maintenance in the permafrost region
13709719909@163.com

Research Paper

Zhang Zhen, Wang Qingzhi, Zhang Kui, Fang Jianhong

Physical and mechanical properties of weathered sandstone rock-like materials under freeze-thaw cycles

Block stone structural layers are commonly utilized in roadbed projects within permafrost areas. However, due to significant temperature fluctuations and frequent freeze-thaw cycles, some of these rock layers have weathered and fractured. Continuous weathering of these rocks results in the block stone embankment gaps becoming clogged, reducing macropore and porous media areas. Consequently, the convective heat transfer function of the block stone roadbed diminishes, failing to adequately protect the frozen soil. This study aims to assess whether recycled weathered rock materials, modified with cement, can match the mechanical properties and damage expansion characteristics of unweathered rocks. Weathered sandstone was selected for modification into rock-like materials. Detailed investigations were conducted into their physical and mechanical properties, alongside damage propagation characteristics following freeze-thaw cycles. Compared to red sandstone, weathered sandstone rock materials exhibit significantly enhanced compressive strength, aligning freeze-thaw damage models with red sandstone rock characteristics, thereby affirming the feasibility of reusing weathered sandstone rocks.

Key words:
physical and mechanical properties, sandstone, freezing and thawing cycles

Prethodno priopćenje

Zhang Zhen, Wang Qingzhi, Zhang Kui, Fang Jianhong

Fizikalna i mehanička svojstva modificiranog trošnog pješčenjaka pri ciklusima smrzavanja i odmrzavanja

Pri projektiranju donjeg ustroja prometnica na području perfmafrosta često se za izvedbu nosivih slojeva koristi blokoviti stijenski materijal. Međutim, uslijed značajnih temperaturnih fluktuacija i čestih ciklusa smrzavanja i odmrzavanja, neki od ovih slojeva se dodatno troše i lome. Kontinuirano trošenje stijenskog materijala dovodi do zapunjavanja praznina u slojevima trupa ceste, smanjujući količinu makropora i veličinu poroznog medija. Posljedično, funkcija konvektivnog prijenosa topline kroz sloj od blokovitog stijenskog materijala smanjuje se te se ne uspijeva adekvatno zaštititi smrznuto tlo. Cilj ovog istraživanja je procijeniti mogu li reciklirani trošni stijenski materijali, modificirani cementom, odgovarati mehaničkim svojstvima i karakteristikama širenja oštećenja netrošnog stijenskog materijala. Trošni pješčenjak odabran je za modifikaciju u materijal sličan stijeni. Provedena su detaljna istraživanja njegovih fizikalnih i mehaničkih svojstava, zajedno s karakteristikama napredovanja oštećenja nakon ciklusa smrzavanja i odmrzavanja. U usporedbi s crvenim pješčenjakom, modificirani trošni pješčenjak pokazuje značajno povećanje tlačne čvrstoće, što usklađuje modele oštećenja uzrokovanih ciklusima smrzavanja i odmrzavanja s karakteristikama crvenog pješčenjaka, čime se potvrđuje mogućnost recikliranja trošnih pješčenjaka.

Ključne riječi:
fizikalna i mehanička svojstva, pješčenjak, ciklusi smrzavanja i odmrzavanja

1. Introduction

China has one of the largest distributions of cold regions globally, with permafrost covering 22.4 % of its land area [1]. The permafrost region in Qinghai Province spans approximately 450,000 sq. km, or 62.5 % of the province [2]. Block stone structural layers are widely used in permafrost regions for subgrade engineering. As depicted in Figure 1 [3], the Gonghe-Yushu high-grade highway, the first of its kind in China, was built in the permafrost region of the plateau. The total length of the block stone subgrades is 55.9 km [4]. Since its inauguration in August 2017, the Gonghe-Yushu high-grade highway's crushed-rock roadbed has experienced varying degrees of irregular settlement, and the pavement has developed transverse and longitudinal fissures, as shown in Figure 2.

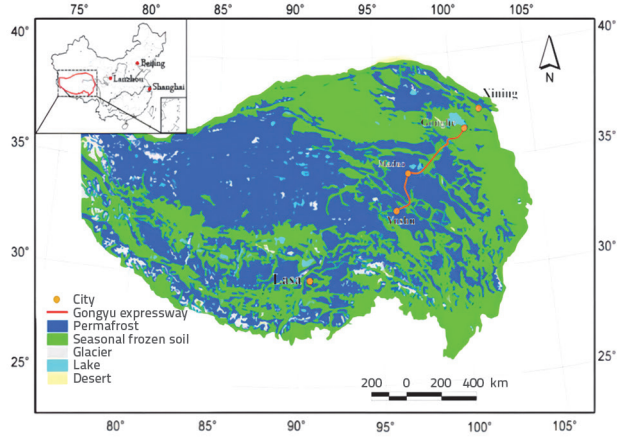

Figure 1. Gonghe-Yushu expressway

The factors contributing to roadbed distress are diverse and complex. A key issue is that block stone roadbeds perform well in low-temperature permafrost areas but poorly in regions with high-temperature permafrost (where temperatures range from 0.0 to -2 °C) [5]. In these areas, the thermal conditions of the high-temperature permafrost beneath the subgrade adversely affect its stability. Unlike typical roads and railways, high-grade highways utilize black asphalt pavements that absorb substantial heat and have wider road widths. This results in increased heat absorption, which intensifies disturbance and impact on the underlying permafrost, thereby raising the likelihood of uneven settlement and roadbed deformation. Additionally, the weathering of stone blocks contributes further to subgrade distress.

Due to frequent freeze-thaw cycles, large temperature variations between day and night, and intense ultraviolet rays on the Qinghai-Tibet Plateau, block stones weather, as illustrated in Figure 3.

Figure 3. Rock weathering on the slope of Gongyu expressway

Weathering reduces the compressive strength of the rocks, making them susceptible to surface cracking and chipping under wind load and human activity. This makes them prone to breakage and significant pore blockage. These issues severely compromise the convection and heat transfer capabilities of block stone slope protection, failing to adequately safeguard the underlying permafrost and leading to subgrade distress. As weathering progresses, accumulated debris further obstructs pores, causing the frozen soil foundation's heat release to melt and settle, resulting in substantial economic losses for engineering projects.

Therefore, recycling these weathered rocks as substitutes for natural aggregates in roadbed construction not only conserves natural resources effectively but also mitigate environmental issues. Furthermore, exploring the feasibility of using weathered rocks in roadbed applications establishes a scientific basis for highway design and construction.

Although there are few domestic and foreign studies on weathered rock as roadbed filler, Zheng et al. [6]

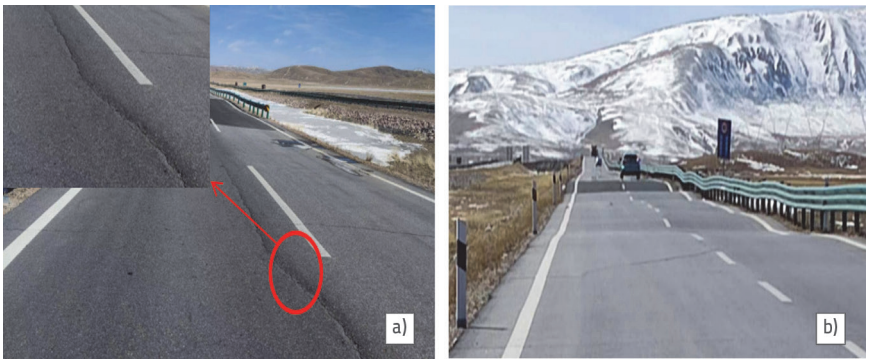

Figure 2. GongYu expressway road condition: a) Longitudinal crack; b) Uneven road settlement

investigated the potential use of weathered soft rock as filling material for subgrades. They considered its mineral composition, disintegration resistance, mechanical strength, and compaction test results, proposing a preliminary approach to assess the suitability of soft rock for subgrade filling. Guo et al. [7] analysed the gradation composition, compaction parameters, and crushing characteristics of four representative weathered rocks. They also studied factors influencing the long-term stability of weathered rock subgrades. Other scholars have explored various properties of weathered rocks. Zhao et al. [8] conducted experimental analysis on the shear strength of fully weathered granite, noting that its deformation and strength characteristics primarily hinge on microstructural traits. Song et al. [9] investigated the deformation and failure patterns of weathered rock in tunnels. Yang et al. [10] employed nuclear magnetic resonance non-destructive testing to detect rock damage and thoroughly analysed the mechanisms of rock damage under freeze-thaw conditions. They found that marble exhibits the highest resistance to rock freeze-thaw weathering, followed by granite and then sandstone, which is in accordance with the law of evolution. Yahaghi et al. [11] studied the physical and mechanical properties of sandstone and its failure behaviour under different freeze-thaw cycle conditions through various indoor tests, including wave velocity experiments, freeze-thaw tests, compressive strength tests, and Brazilian splitting. Li et al. [12] conducted uniaxial and triaxial tests on weathered granite under different temperatures and confining pressures. They believed that temperature and confining pressure have other influence mechanisms on the failure form of weathered granite samples. The reduction of temperature shrinks the mineral particles and the internal microcracks and gaps, thereby increasing the bonding strength. Some scholars have also researched the use of weathered rocks for pavement bases. Felix N et al. [13] studied the stability of cement-stabilized weathered dolomite and its feasibility as a pavement base course through compaction tests and other test results. Xuan et al. [14] reviewed the mechanical properties of cement-stabilized macadam materials and summarized the influence of mixed material parameters on the mechanical properties of cement-stabilized macadam materials. Chen et al. [15] studied the mechanical properties of cement-improved argillaceous slate. They found that the static and dynamic properties have been significantly improved, and the improvement effect is good. Yan et al. [16] assessed the efficacy of cement and lime modifications on weathered argillaceous slate, taking into account factors such as curing conditions, age, and compaction levels. Their findings indicated that lime-treated slate experiences a substantial reduction in strength when immersed in water, in contrast, slate treated with cement demonstrated remarkable stability, unaffected by duration of water exposure. Several researchers have employed materials such as blast furnace slag, steel slag, and fibres for enhancement purposes, achieving outcomes that demonstrate outstanding stability and durability [17-21]. Zhao et al. [22] selected strongly weathered phyllite from the Nanchang area and enhanced it with cement. They studied and analysed the impact of different particle gradation characteristics on the performance of the cement-improved phyllite subgrade filler, verifying the suitability of the enhancement scheme using finite element software. Their research revealed that using cement-modified strongly weathered phyllite as roadbed filler optimises its mechanical properties and permeability, significantly reducing roadbed settlement. This, in turn, extends the service life of the roadbed and the highway's lifecycle. Similarly, Guo et al. [23] demonstrated that cement-treated phyllite exhibited superior compaction properties, resilience modulus, and water stability, with minimal disintegration and improved resistance to disintegration. These enhancements in water stability and disintegration resistance meet the requirements for high-grade highway roadbed construction [24, 25].

In summary, current research focuses on analysing the mechanical properties of weathered rocks and the suitability of modified geomaterials in roadbed construction. Studies indicate that using cement to enhance weathered rock is viable for roadbed filling. However, significant challenges persist in evaluating the durability of these materials under freeze-thaw cycles and in refining methods for recycling and modifying weathered rocks for cold regions. Weathered sandstone serves as the research subject, processed into simulated rock via cement improvement, and subjected to experimental research on its physical and mechanical properties and damage propagation characteristics during freeze-thaw cycles. The aim is to ascertain whether improved recycled weathered rock materials exhibit mechanical properties and damage propagation characteristics comparable to those of unweathered rocks, thereby validating the feasibility of utilising recycled weathered sandstone materials. This research seeks to offer an experimental framework for future applications of recycled weathered rock as roadbed filler.

2. Experimental design

2.1. Overview of the experiment

To investigate the feasibility of using recycled weathered rocks in road construction, this study selected weathered sandstone extracted from the GongYu Expressway as the experimental material. Initially, the weathered sandstone was treated with cement to create rock-like samples. Subsequently, a series of physical and mechanical tests were conducted. By observing and analysing the effects of various freeze-thaw cycles on these modified samples, the study aims to establish links between their macroscopic and microscopic properties. The objective is to assess whether the modified recycled weathered rock material matches the mechanical properties and damage propagation characteristics of unweathered rock, thereby validating the usability of recycled weathered sandstone material.

Table 1. Basic physical parameters of the rock-like sample

Physics parameter	Dry density	Saturated density	Longitudinal wave velocity	Water content	Porosity
Unit	g/cm³	g/cm³	km/s	ω [%]	P [%]
Value	2.31	2.47	4.21	4.70	10.70

2.2. Sample preparation

This investigation utilised samples of weathered sandstone collected from the GongYu Highway construction site and pulverized using a crusher. Weathered sandstone aggregate with particle sizes ranging from 5.0 to 31.5 mm was chosen as the coarse aggregate; the particle size distribution curve is shown in Figure 4. Conventional Portland cement P.O.42.5 from Qinghai and tap water were used as binding materials. The fine aggregate comprised river sand with particle sizes ranging from 0.15 to 4.75 mm, and a naphthalene-based high-efficiency water-reducing agent with a 20 % water-reducing rate was added. The proportions of cement, weathered sandstone aggregate, sand, and water in the mixture were 1:2.72:1.11:0.38, with the admixture dosage set at 1.5 % of the mass of cement. The weathered sandstone was then shaped and cured to form rock-like samples. Following specifications, the cured samples were cut and polished into international standard rock samples measuring 50 mm in diameter and 100 mm in height [26, 27].

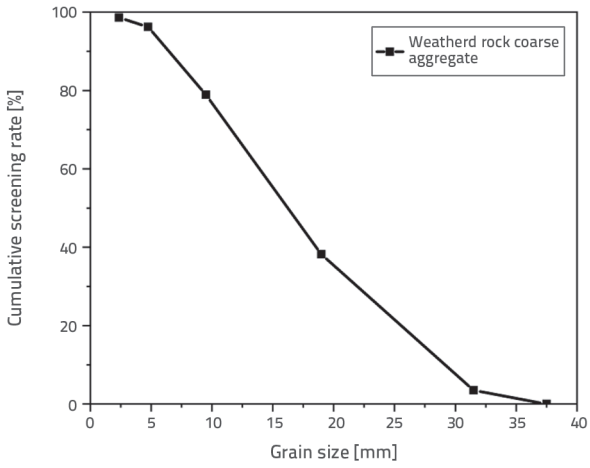

Figure 4. Diagram of the coarse aggregate grading curve

Before testing, specimens showing obvious surface defects were removed. Using the NM-4B non-metallic ultrasonic testing analyser, the P-wave velocity of the remaining specimens was measured to ensure consistency among the 24 specimens selected for the test. These specimens were divided into six groups of four. Subsequently, they were placed in a vacuum saturation apparatus at a pressure of 0.1 MPa for saturation, and their individual weights were recorded. The specimens underwent P-wave velocity measurements at different freeze-thaw intervals and were then evaluated for uniaxial compressive strength under varying freeze-thaw conditions. Table 1 details the fundamental physical characteristics of the weathered sandstone rock-like test specimens.

2.3. Experimental equipment

The freeze-thaw cycle test was conducted using the TMS-9018 freeze-thaw cycle system, which simulates continuous climate changes throughout the year to meet the experiment's precision and stability requirements for the temperature field and provide the necessary temperature environment.

The FRTX-1000 low-temperature, high-pressure, servo-controlled rock triaxial testing system has a maximum axial force of 1000 kN and a confining pressure range of 0 to 2 MPa. The temperature control system can maintain temperatures between -30 °C and 80 °C. The loading rate was 0.05 mm/min.

2.4. Experimental procedure

This study analysed the climate and temperature changes in Maduo County, Qinghai Province, in 2021, revealing temperature fluctuations ranging from -25 °C to 15 °C. To facilitate temperature control and simulate freeze-thaw cycles, the collected temperature data were fitted to a sinusoidal curve. This curve was used to replicate temperature variations in the freeze-thaw cycle chamber, depicted in Figure 5.a. To replicate daily freeze-thaw cycles typical of the region, the sinusoidal curve simulated 12 h of freezing followed by 12 h of thawing.

Further analysis in Figure 5.b indicated that February to April and October to December 2021 experienced more frequent freeze-thaw cycles, averaging nearly 30 cycles per month. Consequently, 0, 5, 10, 15, 20, and 30 freeze-thaw cycles were selected as variables for the experiment, and the samples underwent freeze-thaw cycle testing.

The standard samples of weathered sandstone rock-like material that meet the specifications are placed in an oven and dried at 105 °C for 24 h until a constant weight is attained [28, 29]. Once cooled to room temperature, the samples are taken out, and their mass is measured. These standard samples are then subjected to vacuum-forced saturation in a device maintaining a vacuum pressure of 0.1 MPa, with continuous pumping for 6 h. Subsequently, the samples are saturated in a container for 24 h until no bubbles appear on the surface.

After saturation, the mass of each sample is measured to record its saturated weight. Simultaneously, the height, radius, and P-wave velocity of the samples are determined. These measurements are used to calculate basic physical parameters such as water content, porosity, and density.

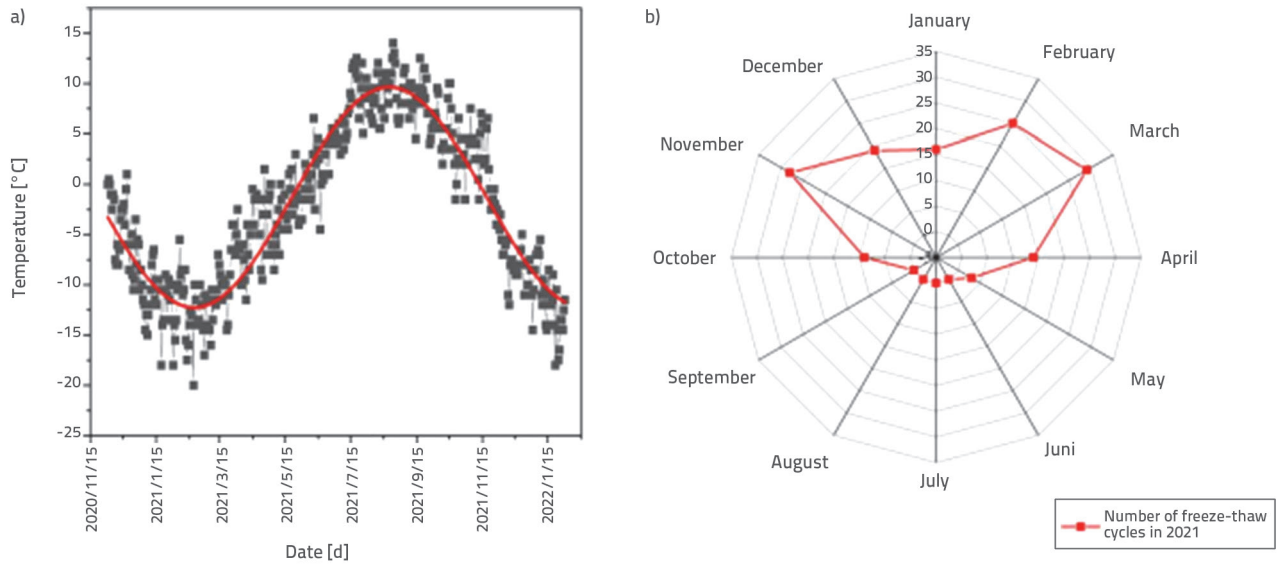

Figure 5. Illustration showing temperature change and freeze-thaw cycles in 2021: a) Temperature trends in 2021; b) Freeze-thaw cycles in 2021

Table 2. The freeze-thaw cycle experimental plan

Parameter	Dry	Saturation time	Freeze-thaw cycles	Freezing and thawing cycle time
Weathered sandstone	24 h	Force saturation for 6 h Standing in water for 12 h	0.5,10,15, 20 and 30 cycles	Freezing time was 12 h Thawing time was 12 h

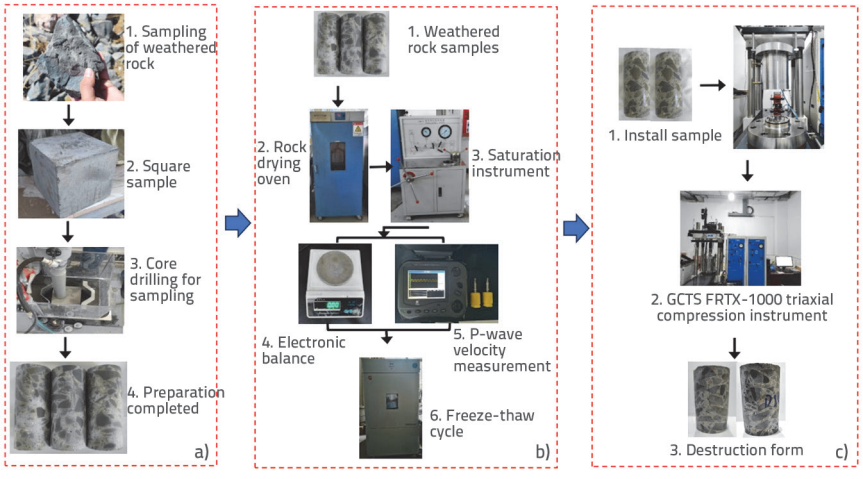

Figure 6. Schematic of the experimental process

Based on these parameters, qualified samples are selected for subsequent freeze-thaw cycle experiments. The freeze-thaw cycle experimental plan is detailed in Table 2.

Once the specified number of freeze-thaw cycles is completed according to the experimental requirements, a uniaxial compression test is conducted, as depicted in Figure 6.

3. Experimental results and analysis

3.1. Changes in the mass of weathered sandstone rock-like samples

For a clearer analysis of the mass and wave velocity changes in the samples, three specimens (WS-1, WS-2, and WS-3) were chosen to observe changes over 30 freeze-thaw cycles. "WS" stands for Weathered Sandstone. The mass change curve of the samples is depicted in Figure 7. It is evident from Figure 7 that the mass of the three groups of freeze-thaw samples increased during the initial five cycles. This increase is primarily attributed to the high porosity of the weathered sandstone rock-like specimens. During freezing, water inside the samples froze and expanded, widening existing fissures and creating new ones due to the force of expansion. During thawing, water seeped into the sandstone rock-like specimens, filling the newly formed fissures and resulting in an increase in sample mass.

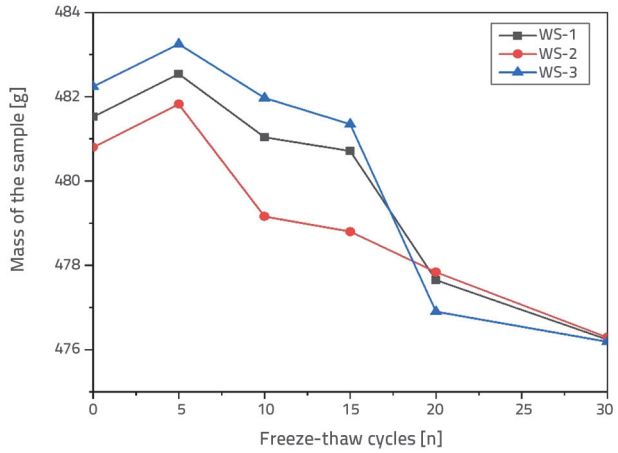

Figure 7. Mass change curve for the sample

After the fifth freeze-thaw cycle, loose particles began to detach from the surface of the specimens, leading to a decrease in sample mass. By the fifteenth cycle, sample mass had decreased further due to loss of aggregates or cementitious material, fractures, and other forms of deterioration, as shown in Figure 8. As the number of cycles increased, the flaking and crumbling of the specimen's surface intensified, resulting in significant declines in sample mass.

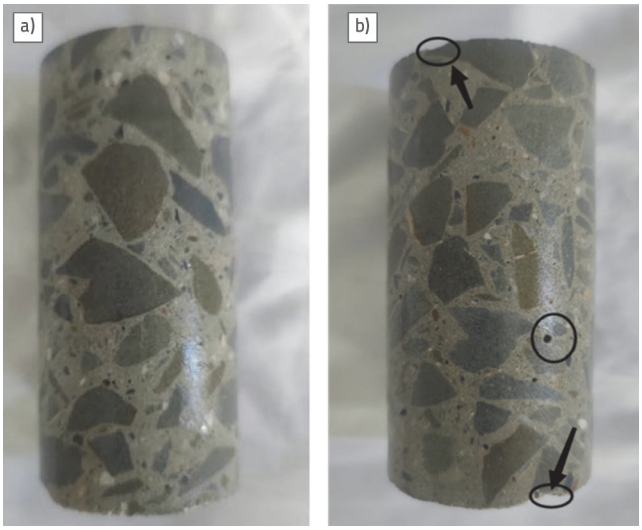

Figure 8. Apparent morphology of rock-like materials under different freeze-thaw cycles: a) 0 freeze-thaw cycles; b) 30 freeze-thaw cycles

3.2. Changes in P-wave velocity

Based on experimental data, Figure 8 depicts the variation curves of wave velocity for the specimens across different freeze-thaw cycle periods. The P-wave velocity decreases as the number of freeze-thaw cycles increases, as illustrated in Figure 9 for the three categories of freeze-thaw samples. Analysis of WS-1 shows that during the initial five freeze-thaw cycles, the specimen's wave velocity decreased by a relatively modest 1.71 %. Subsequent cycles (15, 20, and 30) of freezing and thawing reduced the wave velocity by 8.69 %, 11.46 %, and 18.92 %, respectively. In the other two categories, the rate of change in the sample's wave velocity decreases linearly with increasing freeze-thaw cycles. This is primarily due to the expansion of original cracks within the sample during freeze-thaw cycles, caused by the phase transition of water to ice and uneven shrinkage of aggregates or cement, allowing water to penetrate the sample significantly. The propagation velocity of a wave in water is less than that in the sample, and the wave velocity decreases due to refraction, reflection, and energy loss when traveling through a cracked sample.

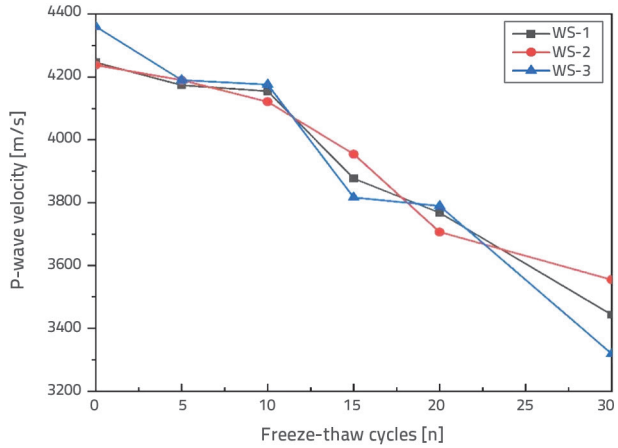

Figure 9. P-wave velocity variation curve

3.3. Stress-strain curves

Figure 10 depicts the uniaxial compressive stress-strain curves of weathered sandstone rock-like samples subjected to different numbers of freeze-thaw cycles.

The uniaxial compressive strength of the weathered sandstone rock-like samples decreases by 39.01 %, from 44.048 MPa at 0 freeze-thaw cycles to 26.863 MPa at 30 freeze-thaw cycles, as depicted in Figure 10.a. Hence, it is evident that the number of freeze-thaw cycles significantly impacts the uniaxial compressive strength of weathered sandstone rock-like materials.

From the analysis of (a) and (b) [30] in Figure 10, it is evident that when the freeze-thaw cycles was zero, the strength of the weathered sandstone rock-like samples was 143.51 % greater than that of the red sandstone rock samples. By the time the freeze-thaw cycles reached 30, the strength of the weathered sandstone rock-like samples exceeded that of the red sandstone rock samples by 125.085 %. Under the same number of freeze-thaw cycles, the uniaxial compressive strength of the weathered sandstone rock-like samples surpasses that of the red sandstone rock samples. This is due to increased adhesion between the weathered sandstone coarse aggregate and cement mortar, reduced pore content within the specimen, improved compactness, and consequently enhanced

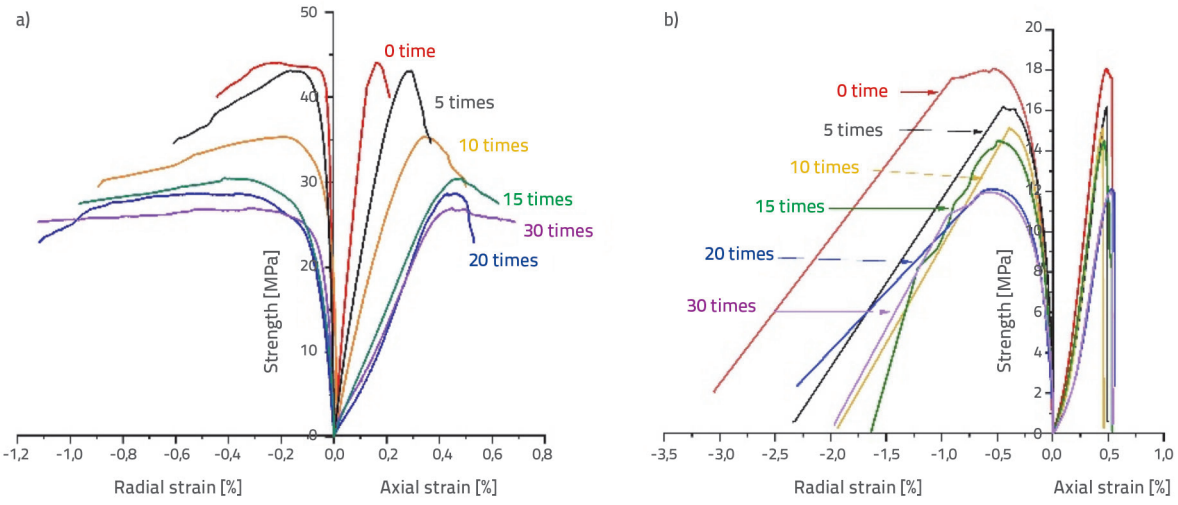

Figure 10. Uniaxial compression stress-strain curve: a) Weathered sandstone rock-like material; b) Red sandstone

compressive strength of the weathered sandstone rock-like samples. Thus, modifying weathered sandstone to resemble rock significantly enhances its compressive strength.

From Figure 10, it is evident that the stress-strain curves of weathered sandstone and red sandstone under varying freeze-thaw conditions exhibit distinct phases from loading to failure: compaction, elastic deformation, plastic yielding, strain softening, and eventual failure. As the number of freeze-thaw cycles increases, the compaction phase of the stress-strain curve becomes more pronounced, the elastic modulus decreases, and both the peak strength and corresponding strain diminish. Concurrently, plasticity continues to increase. In the post-peak region of the stress-strain curve, the rate of stress reduction in weathered sandstone rock-like samples is slower compared to that in red sandstone, indicating a transition from brittle to ductile failure mode in the specimens. Furthermore, Figure 11 illustrates the observed failure modes of the samples.

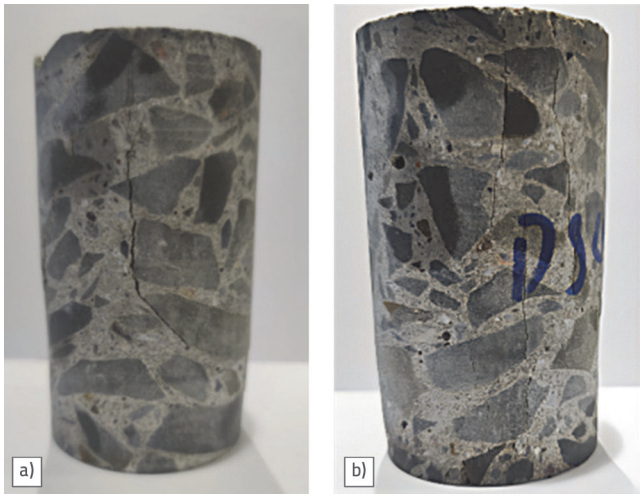

Figure 11. Failure mode of rock-like materials under different freeze-thaw cycles: a) 0 freeze-thaw cycles; b) 30 freeze-thaw cycles

3.4. The variation law of peak strength and elastic modulus

Fitting the points in Figure 12 yielded the following results for the relationship between the number of freeze-thaw cycles and the uniaxial compressive strength and modulus of elasticity.

$$\sigma_w = 25.09 \cdot \exp(-n/19.64) + 20.44 \quad (1)$$

$$\sigma_R = 8.53 \cdot \exp(-n/21.97) + 9.56 \quad (2)$$

$$E_w = 26.63 - 0.94n + 0.031n^2 - 6.3 \cdot 10^{-4}n^3 \quad (3)$$

$$E_R = 4.88 - 0.07n + 0.0012n^2 - 8.4 \cdot 10^{-6}n^3 \quad (4)$$

where σ_W represents the compressive strength (MPa) of the weathered sandstone rock-like samples, σ_R represents the compressive strength (MPa) of the red sandstone samples, E_W represents the elastic modulus (GPa) of the weathered sandstone rock-like samples, E_R represents the elastic modulus (GPa) of the red sandstone samples, and n represents the number of freeze-thaw cycles.

As the number of freeze-thaw cycles increases, the compressive strength of weathered sandstone rock-like samples progressively decreases, as shown in Figure 12.a: 44.048 MPa for 0 cycles, 43.063 MPa for 5 cycles (a decrease of 2.3 %), 35.342 MPa for 10 cycles (a decrease of 19.8 %), 30.454 MPa for 15 cycles (a decrease of 30.9 %), 28.667 MPa for 20 cycles (a decrease of 34.9 %), and 26.9 MPa for 30 cycles (a decrease of 38.9 %). This decrease in strength is due to the formation of fissures and fractures in the cement hydration product, C-S-H gel, as the number of freeze-thaw cycles increases. These pores and fractures impair the bond between the coarse aggregates and cement mortar, resulting in a progressive decrease in the compressive strength of the weathered sandstone rock-like samples exposed to the elements. Although the compressive

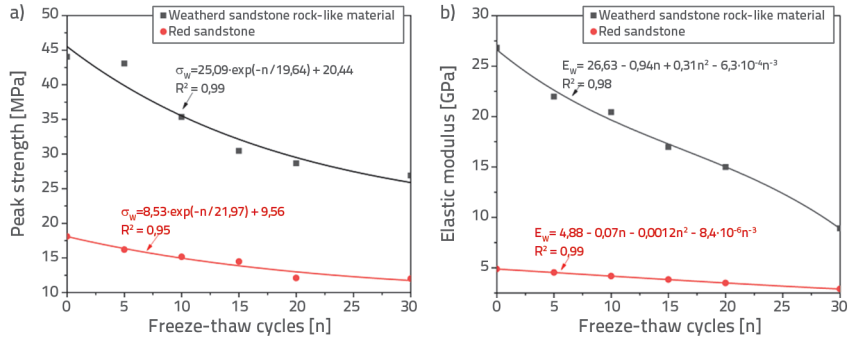

Figure 12. Fitting curves of freeze-thaw cycles with compressive strength and elastic modulus: a) Compressive strength; b Elastic modulus

strength of the weathered sandstone rock-like samples is initially greater than that of red sandstone, the rate of strength loss is higher. Additionally, the fitting formulas reveal a negative correlation between the axial compressive strength and the number of cycles for both sample categories. The strength decreases steadily as the number of cycles increases.

During the freeze-thaw cycle experiment, the damage to the weathered sandstone rock-like samples mirrors that of the red sandstone samples, as both categories sustain comparable damage. This occurs due to the freeze-thaw effect, which allows water to enter the samples through their pores. As the water freezes, it expands, exerting pressure that enlarges internal fissures and develops them into expanding fractures. With each successive freeze-thaw cycle, the bond between aggregates and cementitious material weakens, leading to cumulative damage and reducing the samples' resistance to external forces. Once the freeze-thaw damage reaches a critical threshold, the rock-like samples undergo internal failure, resulting in decreased strength.

Figure 12.b illustrates that the elastic modulus of the weathered sandstone rock-like samples decreases continuously and shows a nonlinear trend with increasing freeze-thaw cycles. Initially, the elastic modulus is 26.814 GPa at 0 cycles. It decreases by 18.02 % at 5 cycles, 23.79 % at 10 cycles, 36.71 % at 15 cycles, 44.12 % at 20 cycles, and 66.74 % at 30 cycles. In contrast, the elastic modulus of the weathered sandstone rock-like samples exhibits a slight increase with the number of freeze-thaw cycles, indicating that these samples are harder and stiffer compared to the red sandstone samples.

The aforementioned experimental findings indicate that the impact of freeze-thaw cycles and external strain on the weathered sandstone rock-like samples is comparable to that on red sandstone. The compressive strength, rigidity, and hardness of the weathered sandstone rock-like samples are significantly greater than those of red sandstone. Various bonding mechanisms, such as physical adsorption, electrostatic interaction, and chemical reactions, occur upon contact between the cementitious material and aggregates. These mechanisms enable the formation of a cohesive structure, thereby enhancing the strength of the sandstone rock-like samples exposed to environmental conditions. Moreover, the hydration reaction of cement plays a crucial role. Cement reacts with water to produce hydrated compounds like calcium silicate and hydrated aluminium, which fill voids between aggregates in the sample. This reduces voids within the aggregates and increases the effective contact area between aggregate particles. Consequently, the bond strength between cement and aggregates is enhanced, contributing to increased sample strength. These interactions collectively augment the strength of the sandstone rock-like samples exposed to environmental conditions.

The frost resistance coefficient quantitatively describes the weathering resistance of sandstone rocks under varying freeze-thaw cycles. It is defined as the ratio of the compressive strength of the sample after each freeze-thaw cycle to that of the water-saturated sample without freeze-thaw. The formula is as follows::

$$K_f = R_f / R_s \tag{5}$$

where R_f represents the compressive strength value (MPa) of the sandstone rock-like samples after freeze-thaw cycles, R_s represents the compressive strength value (MPa) of the sandstone rock-like samples before freeze-thaw cycles, and K_f represents the frost resistance coefficient, which is between 0 and 1.

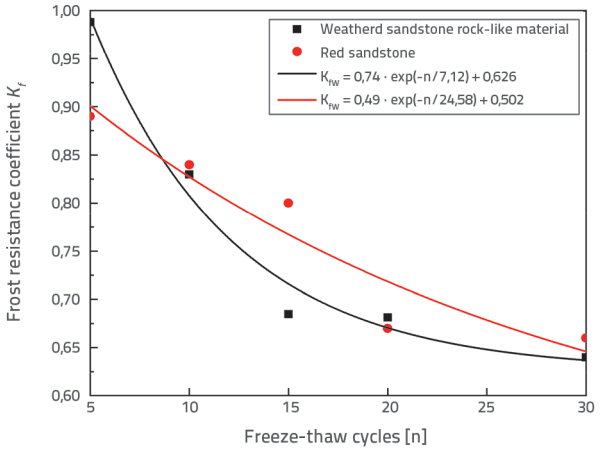

Figure 13. Fitting curve of the frost resistance coefficient and freeze-thaw cycles

Using the above equation, we can establish the characteristic curve of the frost resistance coefficient for weathered sandstone rock-like samples subjected to different numbers of freeze-thaw cycles. This curve is depicted in Figure 13.

The fitting results of the frost resistance coefficient and freeze-thaw cycles were obtained by fitting the points on the curve in Figure 13.

$$K_{fw} = -0.74 \cdot \exp(-n/7.12) + 0.626 \quad (6)$$

$$K_{fR} = -0.49 \cdot \exp(-n/24.58) + 0.502 \quad (7)$$

K_{fW} and K_{fR} represent the freezing resistance coefficients of the weathered sandstone rock-like specimens and red sandstone, respectively.

From the analysis of the fitted curves and equations, it is clear that the frost resistance coefficients of the weathered sandstone rock-like specimens vary with the number of freeze-thaw cycles, indicating that these specimens experience varying degrees of freeze-thaw damage over different cycle times. As shown in Figure 12, both the weathered sandstone rock-like specimens and the red sandstone exhibited a progressive decrease in frost resistance coefficients as the number of freeze-thaw cycles increased, with a sharp decline in the first 20 cycles followed by gradual stabilisation. This demonstrates that freeze-thaw action significantly impacts weathered sandstone rock-like samples.

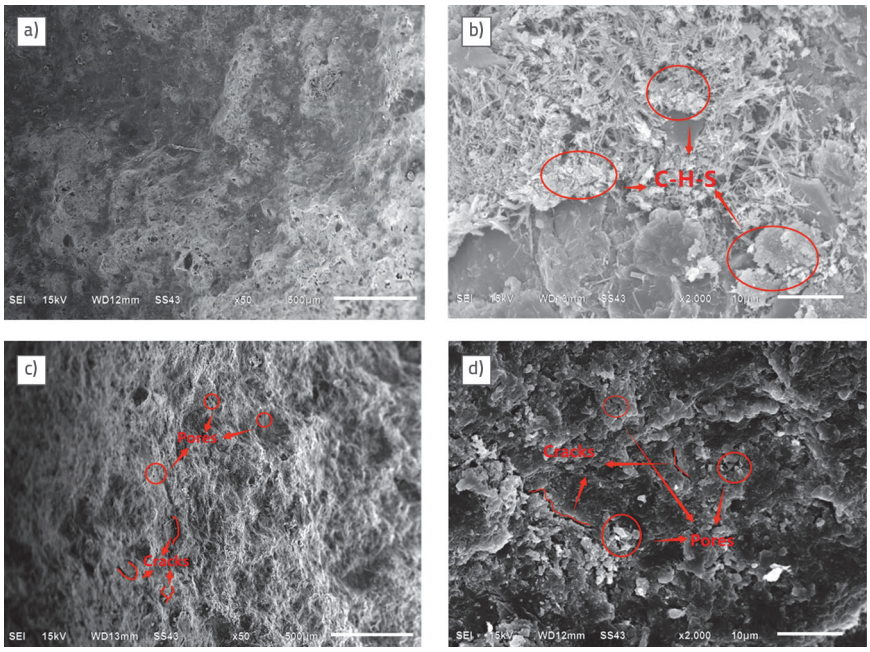

Figure 14. Scanning electron microscopy images of weathered sandstone rock-like material: a) 0 freeze-thaw cycles of 50 x; b) 0 freeze-thaw cycles of 2000 x; c) 30 freeze-thaw cycles of 50 x; d) 30 freeze-thaw cycles of 2000 x

4. Study on microscopic damage of the weathered sandstone under freeze-thaw environment

To explore the impact of freeze-thaw cycles on the microstructure of weathered rock-like samples, this study conducted electron microscope scanning experiments on samples subjected to various freeze-thaw cycles. It is evident from the results that the compressive strength of the sample undergoes significant changes after 0 and 30 freeze-thaw cycles. Figure 13 illustrates the microstructure of weathered sandstone rock-like samples under different numbers of freeze-thaw cycles.

The internal structure of weathered sandstone before freeze-thaw cycles is dense and uniform, with few fissures, as depicted in Figures 14.a and 14.b. The C-S-H gel appears flocculent and flake-shaped, containing rod-like structures. Within the rock-like samples, these rod-like and flocculent structures intertwine and are embedded in a grid or honeycomb pattern, with some pores filled by the product. The structure is solid, compact, and devoid of visible fractures.

In contrast, as depicted in Figures 14.c and 14.d, the weathered sandstone rock-like formations exhibit numerous fissures and cavities. The pore structure is larger and more porous, with a relatively disorganised arrangement and an enriched flocculent C-S-H gel. However, the presence of numerous gel pores and the development of microcracks adversely affect the strength of weathered sandstone rock-like materials.

The PCAS software was employed to quantitatively analyse the porosity and average perimeter of electron microscope images of weathered sandstone rock-like samples. Figure 15 illustrates the relationship between porosity, average perimeter, and the number of freeze-thaw cycles.

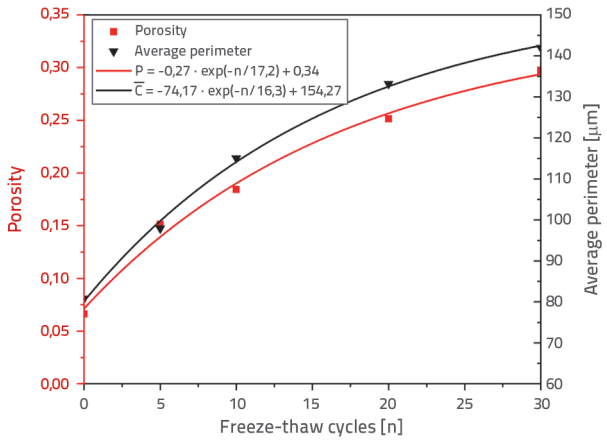

Figure 15. Pore volume, average pore size, and the fitting curve of freeze-thaw cycles

By fitting the data points in Figure 15, the fitting results for porosity (P), average perimeter ($\bar{C}$), and several freeze-thaw cycles (n) can be obtained as follows:

$$P = -0.27 \cdot \exp(-n/17.2) + 0.34 \quad (8)$$

$$C = -74.17 \cdot \exp(-n/16.3) + 154.27 \quad (9)$$

As the number of freeze-thaw cycles increases, the porosity of weathered sandstone rock-like samples also increases, causing their internal structure to become progressively more porous with larger, rounder fissures. Moreover, the number of apertures increases. Additionally, the average perimeter of the pores increases gradually with the number of freeze-thaw cycles, indicating that small pores develop and expand during these cycles. Water molecules freeze and expand during freeze-thaw cycles, causing the pores and fissures to develop in multiple directions. This expansion process enlarges the pores, leading to their gradual merging and fusion. At a macroscopic level, the specimen's damage worsens progressively, and particles gradually detach, resulting in reduced strength.

Both findings indicate that pore water within weathered sandstone rock-like samples generates significant frost heave forces within the pores during freezing. This process results in the disintegration of the structure surrounding the pores and a gradual increase in porosity. Furthermore, the results of the microstructure analysis of the weathered sandstone rock-like material before and after the freeze-thaw process align with the observed changes in compressive strength.

5. Damage propagation characteristics of freeze-thaw loaded rock

A damage constitutive model for weathered sandstone rock-like material under freeze-thaw loading was developed using damage mechanics mechanisms and experimental data on the strength and mechanical properties of the material after freeze-thaw cycles.

5.1. Constitutive relationship of rock under freeze-thaw and load

There are currently three representations of the damage variable D due to the different forms and numbers of damage to rock materials. However, as the number of freeze-thaw cycles increases, the phase transition of water and ice within the rock and the uneven expansion and contraction of minerals lead to the continuous generation and increase of new cracks. Macroscopic physical quantities respond accordingly. Therefore, the change in elastic modulus can be used to measure the degree of damage to the rock, and its freeze-thaw damage variable is defined as follows:

$$D_n = 1 - (E_n/E_0) \quad (10)$$

where E_0 is the initial elastic modulus of the rock prior to freezing and thawing. E_n is the elastic modulus of the rock after n freeze-thaw cycles.

Since most rocks already have initial damage, the damage state of frozen-thawed rock is defined as the base damage state, following Lemaitre's strain equivalence principle [30-33]. The generalized strain equivalence principle is proposed as follows:

$$\sigma = E\varepsilon(1-D) \quad (11)$$

where E is the elastic modulus of the nondestructive material, and D is the load damage variable.

The first damage state occurs after freeze-thaw damage, while the second damage state reflects the cumulative freeze-thaw burden damage. Therefore, to establish the connection between freeze-thaw damage and internal damage:

$$\sigma = E_n\varepsilon(1-D) \quad (12)$$

where E_n is the rock's elastic modulus after freezing and thawing.

Eqs. (10) and (12) can be used to calculate the stress-variation relationship induced by the rock freeze-thaw load, represented by the rock freeze-thaw load damage variable.

$$\sigma = E_0\varepsilon(1-D_m) \quad (13)$$

$$\text{One of } D_m = D + D_n - DD_n \quad (14)$$

where D_m is the total damage variable of the rock subjected to the freezing and thawing loads.

Equation (14) shows that the combined effects of freezing, thawing, and loading increase granite damage. The coupling term illustrates, through a fundamental analysis of freeze-thaw damage, that the dual-stage coupling action exacerbates total damage and affects the internal microstructure. Upon loading, the closed microparticles within the rock adhere tightly to each other, exhibiting significant nonlinearity in their characteristics and reducing overall damage.

5.2. Damage evolution law of freeze-thaw loaded rock

Under loading, the specimen can be viewed as a field of damage. Internal defects within the specimen continue to develop and expand, leading to a progressive decline in strength. This damage continues until failure occurs during the loading process. As the load accumulates, each micro-element of its internal structural defects is broken down into numerous elements, introducing randomness and complexity to the failure of micro-elements within the sample.

From a damage perspective, the specimen under load can be seen as a field of damage. Internal defects within the specimen continue to develop and expand, resulting in a continuous decline in strength. This process continues until the specimen fails under stress. As the burden progressively accumulates, each micro-element of its internal structural defects is discretised into multiple elements. The failure of these micro-elements within the sample is random and complex. Assuming the strength of the micro-element follows a Weibull distribution function, the probability density function of the micro-element's failure can be expressed as follows:

$$P(\varepsilon)=\frac{m}{\lambda}\left(\frac{\varepsilon}{\lambda}\right)^{(m-1)}e^{-\left(\frac{\varepsilon}{\lambda}\right)^{m}} \quad (15)$$

where ε is the strain of the micro-unit. P (ε) is the distribution function of the micro-unit. m and λ are the two parameters of the Weibull statistical distribution.

The failure of the material is equivalent to a large amount of damage to the microelement strength of the rock. The damage variable of the rock under load is defined as the ratio of the number of damaged micro-elements n_1 to the total number of material micro-elements N, namely: $D = n_1/N$. The number of elements destroyed in any interval [ε, ε + dε] is NP (ε) dε, then:

$$D=\frac{n_1}{N}=\frac{\int_0^{\varepsilon}NP(\varepsilon)d\varepsilon}{N}=1-e^{-\left(\frac{\varepsilon}{\varepsilon_\lambda}\right)^{m}} \quad (16)$$

where ε_λ is the strain value corresponding to the peak value σ_λ and m is the material parameter characterising the damage evolution characteristics of materials, $m = 1/\ln(E_0\varepsilon_\lambda/\sigma_\lambda)$.

Eqs. (10), (14), and (16) can be used to calculate the control variables of damage evolution when the strain and number of freeze-thaw cycles are used as control variables:

$$D_m=1-\frac{E_n}{E_0}e^{-\left(\frac{\varepsilon}{\varepsilon_\lambda}\right)^{m}} \quad (17)$$

Eq. (13) can be used to determine the evolution equation of the overall damage rate of rock when the strain and number of freeze-thaw cycles change.

$$D_m=(1-D_n)\frac{\partial D}{\partial \varepsilon}+(1-D)\frac{\partial D_n}{\partial n} \quad (18)$$

According to the strain equivalence principle proposed by Lemaitre, the constitutive model of rock damage under normal conditions is as follows:

$$\sigma=E_0\varepsilon(1-D_m)=E_n\varepsilon e^{-\left(\frac{\varepsilon}{\varepsilon_\lambda}\right)^{m}} \quad (19)$$

The damage progression curve of weathered sandstone rock-like material under freeze-thaw stress is calculated using Eq. (17), based on the test findings from Figure 10, and is depicted in Figure 16.

Under the same number of freeze-thaw cycles, Figure 16 shows that freeze-thaw damage to weathered sandstone rock-like material and red sandstone deteriorates significantly as the cycles increase. Up to the first 15 cycles, the trend lines of the damage variables for both samples are nearly identical, showing a gradual decline in intensity. However, between 15 and 30 cycles, the damage variable of the weathered sandstone rock-like material shows a slow increase followed by a sharp rise, whereas that of the red sandstone shows a rapid increase followed by a slower rise. Beyond a certain number of freeze-thaw cycles, the rate of freeze-thaw damage to weathered sandstone rock-like material increases.

During the initial loading stage, the original internal fractures and new microcracks generated by freeze-thaw gradually close and weaken under pressure. As the load increases, the rate of deterioration accelerates, with microcracks continuing to form and connect, eventually leading to macrocracks. Once deformation reaches a set threshold, damage begins to evolve, expanding steadily until it accelerates and approaches a damage variable of 1. After reaching its peak, the rate of damage to the sample under sustained loading progressively decreases. This shift occurs because the sample transitions from brittle to plastic after sustaining damage, slowing down the rate of damage under stress until the damage variable approaches 1.

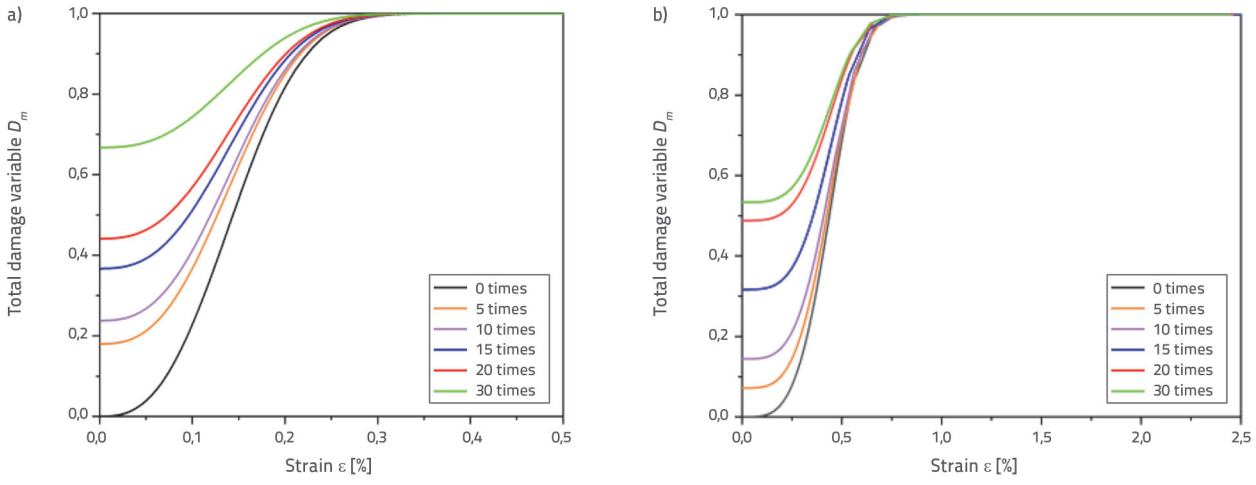

Figure 16. Damage evolution curve:) Weathered sandstone rock-like material; b) Red sandstone

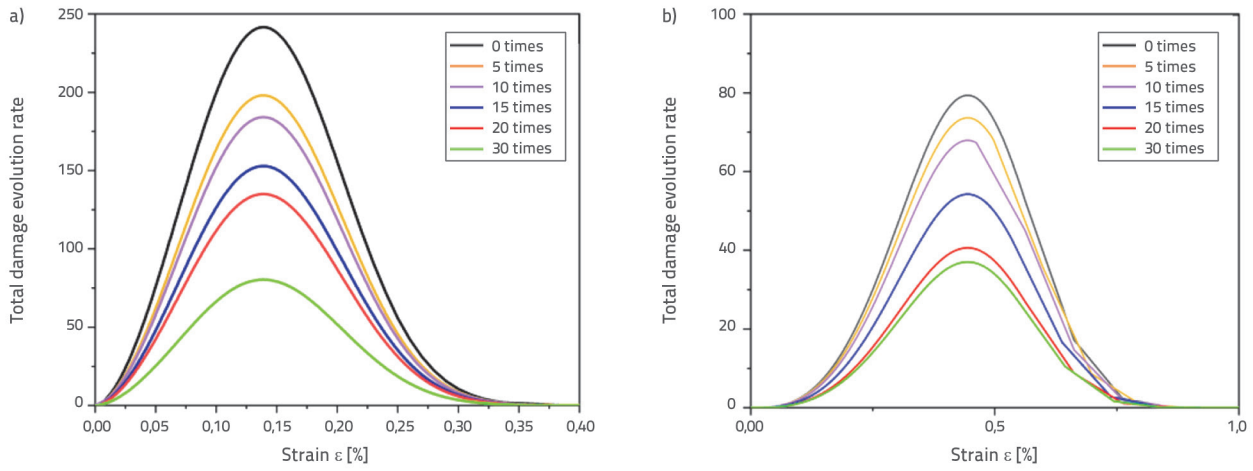

Figure 17. Total damage rate evolution curve: a) Weathered sandstone rock-like material; b) Red sandstone

Using Eqs. (10), (16), and (19), Figure 17 depicts the total damage rate evolution curve of weathered sandstone rock-like material.

Figure 17 shows that, under the same freeze-thaw cycles, the damage rate of weathered sandstone rock-like material and red sandstone increases with strain and decreases steadily after reaching a peak. At equivalent strain levels, the rate of damage evolution for both samples decreases progressively as the number of freeze-thaw cycles increases, indicating a continuous increase in their plasticity. The area under the damage evolution rate curve in Figure 17 represents the total damage variable D_m. The damage characteristics observed in weathered sandstone rock-like material and red sandstone are consistent with those shown in Figures 16 and 17. Moreover, the damage propagation behaviour of weathered sandstone rock-like material under freeze-thaw cycles aligns with the predicted variations in rock mechanical behaviour as revealed by the freeze-thaw load damage model, corroborating the findings and analytical conclusions drawn from mechanical characteristic tests conducted on samples subjected to freeze-thaw cycles.

6. Conclusion

The following conclusions can be drawn from this study:

Freeze-thaw cycles significantly reduce the resistance of weathered sandstone rock-like materials to external loads. These cycles induce microcracks, loss of aggregate or cement, and fractures in weathered sandstone rock-like materials. Initially, the mass of the sample slightly increases with the number of freeze-thaw cycles before decreasing. Furthermore, the P-wave velocity consistently decreases as the number of freeze-thaw cycles increases.

The compressive strength of weathered sandstone rock-like materials decreases with an increasing number of freeze-thaw cycles. In comparison to red sandstone, weathered sandstone rock-like materials exhibit a notably higher compressive strength. This increase can be attributed to the hydration products formed from the reaction between cement and aggregates, which fill the gaps within the weathered sandstone aggregates. This reduces void spaces, increases the effective contact area between aggregate particles, and enhances the cementitious strength.

Scanning electron microscopy provides insight into the internal structure and porosity changes of weathered sandstone rock-like material under different freeze-thaw cycles. As the number of cycles increases, the porosity of the weathered sandstone rock-like material increases, its internal structure loosens, and the shapes of its pores enlarge while their number grows. Consequently, the average perimeter of the pores gradually increases, leading to the progressive interconnection of pores and a reduction in the strength of weathered sandstone rock-like material.

The establishment of a freeze-thaw damage model reveals that the damage to weathered sandstone rock-like material is exacerbated by the combined effects of freeze-thaw cycles and loading. This finding aligns with the damage variation characteristics observed in red sandstone rock, further validating the applicability of weathered sandstone rock-like material.

Acknowledgments

This work was supported by the National Natural Science Foundation of China (No. 42161026 & 41801046), the Science and Technology Plan Project of Qinghai Province (No. 2023-QY-206), and the Youth Research Foundation of Qinghai University (No. 2022-QGY-5).

REFERENCES

[1] Zhou, Y., Guo, D., Qiu, G., et al.: Geocryology in China. Beijing: Science Press, 2000.

[2] Xu, X., Wang, J., Zhang, L.: Frozen soil physics. Science Press, 2010.

[3] Wang, Q., Fang, J., Zhao, X., et al.: The influence of pavement type on the thermal stability of block-stone embankments in the warm permafrost region. Transportation Geotechnics, 23 (2020) 11, pp.100334.

[4] Wang, Q., Fang, J., Chao, G., et al.: Analysis of the cooling effect of high grade highway block stone subgrade in high temperature frozen soil area. Rock and Soil Mechanics, 41 (2020) 1, pp. 305-314.

[5] Xu, Y., Shen, M., Zhou, Z., et al.: Study on long-term thermal stability of typical subgrade in high temperature permafrost region of Qinghai-Tibet Railway. Journal of Glaciology and Geocryology. 44 (2022) 06, pp. 1784-1795.

[6] Zheng, M., Fang, T., Diao, X., et al.: Laboratory test on the feasibility of filling roadbed with weathered soft rock. Geotechnical mechanics, S1 (2005), pp. 53-56.

[7] Guo, Y., Shen, A., Gao, T., et al.: Road performance test and weathering degree evaluation of weathered rock roadbed filler. Journal of Transportation Engineering, 2014, 14 (2014) 3, pp. 15-23.

[8] Zhao, J., Wang, S., Shang, Y., et al.: Analysis of Influencing Factors on Shear Strength of Completely Weathered Granite. Geotechnical Mechanics, 4 (2005), pp. 624-628.

[9] Ki-Il, S., Gye-Chun, C., Seok-Won, L.: Effects of spatially variable weathered rock properties on tunnel behavior. Probabilistic Engineering Mechanics, 26 (2010) 3.

[10] Yang C, Zhou K, Xiong X, et al.: Experimental investigation on rock mechanical properties and infrared radiation characteristics with freeze-thaw cycle treatment. Cold Regions Science and Technology, 183 (2021), pp.103232.

[11] Yahaghi, J., Liu, H., Chan, A., et al.: Experimental and numerical studies on failure behaviours of sandstones subject to freeze-thaw cycles. Transportation Geotechnics, 31 (2021), pp. 100655.

[12] Li, J., Li, G., Peng, W., et al.: Analysis of the strength and deformation characteristics of saturated water weathered granite under different temperature conditions. Journal of Glaciology and Geocryology, 42 (2020) 2, pp. 23-531.

[13] Felix, N., Okonta Oluwapelumi, O.O.: The Stabilization of Weathered Dolerite Aggregates with Cement, Lime, and Lime Fly Ash for Pavement Construction. Advances in Materials Science and Engineering, 2014, pp. 11.

[14] Xuan, D., Houben, L., Molenaar, A., et al.: Mechanical properties of cement-treated aggregate material-A review. Materials & Design, 33 (2012) 1, pp. 496-502.

[15] Chen, L., Zhang, J., Chen, J., et al. Static and dynamic characteristics test of cement-improved argillaceous slate coarse-grained soil. Geotechnical mechanics, 38 (2017) 7, pp. 1903-1910.

[16] Geçkil, T., Tanyıldızı, M.M., İnce, C.B.: Investigation of Use Potential of Fiber Added Concretes as Road Pavement on Weak Soils, GRAĐEVINAR,75 (2023) 7, pp.665-678, https://doi.org/10.14256/JCE.3619.2022.

[17] Es-Samlali, L., Haloui, Y. E., Amrani, M., Oudrhiri-Hassani, F., Tlidi, A., Bekri, A.: Potential valorisation of steel slag waste as an alternative material for pavement layers, GRADEVINAR, 75 (2023) 2, pp. 163-176, https://doi.org/10.14256/JCE.3571.2022.

[18] Geçkil, T., Tanyıldızı, M.M., İnce, C.B.: Benefit–cost relationship of using concrete with blast furnace slag as road pavement, GRADEVINAR, 75 (2023) 1, pp. 23-37, https://doi.org/10.14256/JCE.3570.2022.

[19] Karadag, H., Fırat, S., Işık, N.S., Yılmaz, G.: Determination of permanent deformation of flexible pavements using finite element model, GRADEVINAR, 74 (2022) 6, pp.471-480, https://doi.org/10.14256/JCE.2708.2019.

[20] Kulkarni, S., Ranadive, M.: Effect of soil stabilization on design of conventional and perpetual pavement in India, GRAĐEVINAR, 74 (2022) 9, pp. 779-787, https://doi.org/10.14256/JCE.3337.2021.

[21] Yan, G., Li, L., Shu, H., et al.: Experimental study on unconfined compressive strength of fully weathered argillaceous slate improved soil. Geotechnical Engineering,12 (2009) 7, pp. 73-76.

[22] Zhao, Y., Li, Y., Wang, C., et al.: Road performance of ordinary Portland cement improvement of strongly weathered phyllite filler. Construction and Building Materials, 350 (2022), pp. 128801.

[23] Guo, Z., Ji, X., Wang, Y., et al.: Cement modified phyllite roadbed filler test. China Science and Technology Paper, 17 (2022) 7, pp. 724-730.

[24] Wei, S., Wang, C., Yang, Y., et al.: Physical and mechanical properties of gypsum-like rock materials. Advances in Civil Engineering, 2020 (2020), pp. 1-17.

[25] Wu, Y., He, Q., Wang, Y.: Creep characteristics of rock-like materials under freeze-thaw cycles. Industrial building, 50 (2020) 10, pp. 106-110+62.

[26] Changjiang Academy of Science: Code for rock tests in water and hydro power projects, SL/T264-2020, Ministry of Water Resources of the People's Republic of China, 2020.

[27] Ministry of Transport of China: Test Methods of Rock for Highway Engineering. People's Transportation Publishing House, 2017.

[28] Selen, L, Panthi, K.K., Vistnes, G.: An analysis on the slaking and disintegration extent of weak rock mass of the water tunnels for hydropower project using modified slake durability test. Bulletin of Engineering Geology and the Environment, 79 (2020), pp. 1919-1937.

[29] ISRM: Suggested methods for determining water content, porosity, density, absorption and related properties and swelling and slakedurability index properties: Part 1: suggested methods for determining water content, porosity, density, absorption and related properties. Int J Rock Mech Min Sci Geomech Abstr 16 (1979) 2, pp. 143-151.

[30] Zhang, Q., Wang, Q., Fang, J., et al.: Study of the characteristics mechanical damage and constitutive model of crushed-rocks from high-grade highway in permafrost region. Geofluids, 2022 (2022), pp. 1-17.

[31] Zhang, Q., Yang, G., Ren, J.: New discussion on damage variable and constitutive equation of rock. Chinese Journal of Rock Mechanics and Engineering,22 (2003) 1, pp. 30-34.

[32] Yuan, X., Liu, H., Liu, J.: A damaging model of jointed rock under coupled action of freezing and the wing. Journal of Rock Mechanics and Engineering,34 (2015) 8, pp. 1602-1611.

[33] Xu, W., Wei, L.: Research on statistical constitutive model of rock damage. Chinese Journal of Rock Mechanics and Engineering, 21 (2002) 6, pp. 787-791.